frontiers | Frontiers in Earth Science

TYPE Original Research
PUBLISHED 25 October 2023
DOI 10.3389/feart.2023.1220173

OPEN ACCESS

EDITED BY
Idoia Rosales,
CN Instituto Geológico y Minero de España (IGME, CSIC), Spain

REVIEWED BY
Jerzy Dzik,
Polish Academy of Sciences, Poland
Josefina Carlorosi,
Instituto Superior de Correlación Geológica (INSUGEO), Argentina

*CORRESPONDENCE
Xueying Ma,
752032397@qq.com

RECEIVED 10 May 2023
ACCEPTED 18 September 2023
PUBLISHED 25 October 2023

CITATION
Ma X, Deng S, Lu Y, Fan R, Zhang F, Sun Y, Li X and Qu Z (2023), Using chemostratigraphy and biostratigraphy methods to define the unconformity underlying the Upper Ordovician Pagoda Formation in the Upper Yangtze Platform. *Front. Earth Sci.* 11:1220173. doi: 10.3389/feart.2023.1220173

Using chemostratigraphy and biostratigraphy methods to define the unconformity underlying the Upper Ordovician Pagoda Formation in the Upper Yangtze Platform

Xueying Ma[1]*, Shenghui Deng[1], Yuanzheng Lu[1], Ru Fan[1], Fenglian Zhang[2], Yanqi Sun[1], Xu Li[3] and Zhengyang Qu[4]

[1]Research Institute of Petroleum Exploration and Development, PetroChina, Beijing, China, [2]School of Ocean Sciences, China University of Geosciences, Beijing, Beijing, China, [3]No.4 Gas Production Plant, PetroChina Changqing Oilfield Company, Ordos, Shanxi, China, [4]No.4 Oil Production Plant, PetroChina Changqing Oilfield Company, Yinchuan, Ningxia, China

The discovery of hydrocarbon in the Pagoda Formation in South China has received attention from the petroleum industry. This research paper identifies the discontinuity surface underlying the Pagoda Formation. The Upper Ordovician strata were correlated in different regions using the conodont biostratigraphy, and $\delta^{13}C$ and $\delta^{18}O$ isotope stratigraphy. The biostratigraphic result illustrates that three conodont zones can be established in each study section, and one to three conodont zones are missing in the lower Pagoda Formation and the strata underlying the Pagoda Formation of the Upper Yangtze Platform. Moreover, the chemostratigraphic result highlighted that the development of the lower $\delta^{13}C$ isotope positive excursion events in the Xiaogangwan and Liangcun areas was less complete than that in the Jiaodingshan area. Combined with the cyclostratigraphic results, the development of the $\delta^{13}C$ isotope positive excursion is not complete. The development of the $\delta^{13}C$ excursion event is more complete in the south and east than in the center and north. This demonstrates that the Pagoda Formation began its deposition at different times and the transgression process may have advanced from the southeast to the north and that the contact between the Pagoda Formation and the underlying formation is not conformable. It is proposed that the Late Ordovician in the South China Plate was affected by the tectonic movement and the cooling paleoclimate at that time, which resulted in the discontinuity between the Pagoda Formation and the underlying strata. The unconformity could be the channel for hydrocarbon migration or for the high-quality oil and gas reservoirs being developed and preserved under the unconformity surface.

KEYWORDS

carbon and oxygen isotope, conodont, unconformity, Pagoda Formation, Upper Ordovician, Upper Yangtze Platform

1 Introduction

South China is one of the most well-known areas developing the Ordovician strata (Sheng and Ji, 1984; An et al., 1985; Sheng and Ji, 1986; Mu et al., 1987; Wang Y. Y. et al., 2018). Many investigations were carried out on the Ordovician strata (Wei et al., 2017; Peng et al., 2018; Li et al., 2022; Wan et al., 2022), especially in the Middle-Lower Yangtze Platform (An, 1987; Wang and Ni, 1987; Chen et al., 1997; Rong et al., 2000). Not only was the Ordovician chronostratigraphic attribution determined, but the Global Boundary Stratotype Section and Point with three Ordovician stages were also established (An et al., 1981; Lin et al., 1984; Zhao et al., 2006). The Ordovician strata were most extensively developed in the Upper Yangtze Platform, especially in the Sichuan Basin. With the advancement and breakthrough of the Paleozoic oil and gas exploration in the Upper Yangtze Platform, the unconformity surface of the Ordovician stratigraphy and the area have been attracting more and more attention in the geoscience field in the last few decades. Unconformity surfaces are effective channels for hydrocarbon accumulation and migration, and many large and super-large scale oil fields in the world are related to them.

The conodonts are excellent Paleozoic biostratigraphic tools and the study of the Ordovician conodonts in the Sichuan basin has provided an important basis for the division and correlation of related strata (Sepkoski and Sheehan, 1983; Jiang and An, 1985; An, 1987; An and Zheng, 1990; Chen, 1994; Wang et al., 2017). However, the biostratigraphic correlation of conodonts in the western part of the Upper Yangtze Platform is sparse, and the accuracy of stratigraphic division can be improved. The outcrops of the Jiaodingshan section of Hanyuan, Yaan, Sichuan Province, in the western part of the Upper Yangtze Platform, are well exposed, making it an ideal section for the study of Late Ordovician conodont biostratigraphy. The Middle-Upper Ordovician strata of the Sanquan section of the Nanchuan, Chongqing, and the Hongyan section of the Xikou, Huaying, Sichuan, located in the eastern and central portion of the Upper Yangtze Platform, are continuously developed and could be chosen to correlate with the strata of the Jiaodingshan section in the western portion.

The main purpose of this research paper is to contribute to the chemostratigraphic and biostratigraphic study of the Middle-Upper Ordovician Pagoda Formation based on carbon and oxygen isotopes and conodont specimens; determining their age and contact relationship. This research will be a good reference for future oil and gas exploration in the area.

2 Geological setting

China consisted of three plates in the Ordovician, namely, North China, South China, and Tarim (Figure 1A). The Yangtze Platform, located in the northwestern part of South China, is recognized as a small craton that represents the area of Ordovician major strata distribution in South China. Moreover, the Yangtze Platform is characterized by shallow marine deposition, and it evolved to slope and basin environments at the end of the Ordovician, with the corresponding water deepening. The Yangtze Platform is divided into the Upper Yangtze Platform and the Middle-Lower Yangtze Platform with the boundary of Jiangxi province. The study area of this research is located in the Upper Yangtze Platform, where the Ordovician limestone and mudstone and a large number of fossils were discovered, including ostracoda, graptolite, and conodonts. The continuous conodont zones from the Yichang area (located in the Middle-Lower Yangtze Platform) were used to correlate related strata.

2.1 Study sections and lithology

Three sections were analyzed in this study, namely, the Jiaodingshan section, the Sanquan section, and the Hongyan section, which are widely spread all over the Upper Yangtze Platform. The Jiaodingshan section spreads into the Malie, Hanyuan, Yaan, and Sichuan provinces and is located 67 km northeast of the Hanyuan government office (102.87N, 29.4E) (Figure 1B). The Jiaodingshan is the eastern remnant of the Daxiangling Mountain Range, which shows a north-south trend

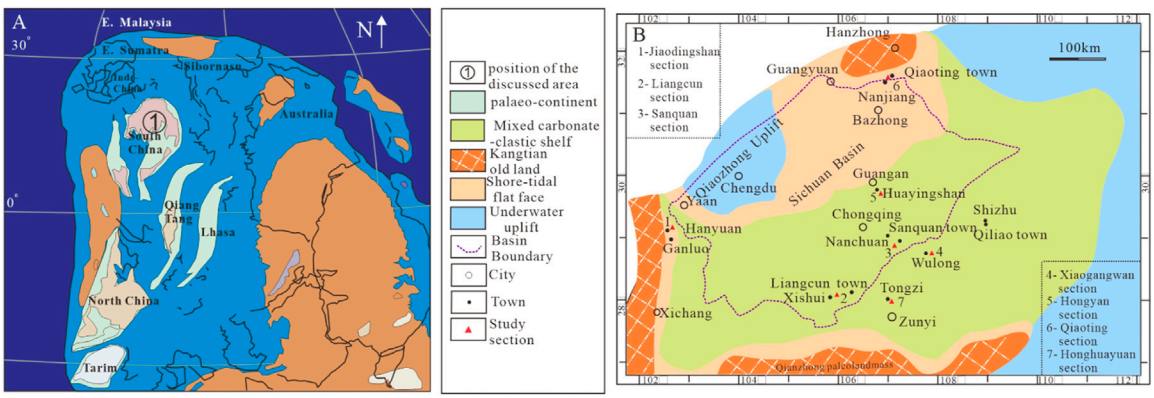

FIGURE 1
Late Ordovician paleogeography of South China and the location of the discussed sections in the Sichuan Basin. **(A)** Geographic location of South China in late Ordovician, which is modified after Ogg et al. (2019); **(B)** Geological sketch-map of the Sichuan Basin showing the location of the discussed outcrops (Ma et al., 2019a).

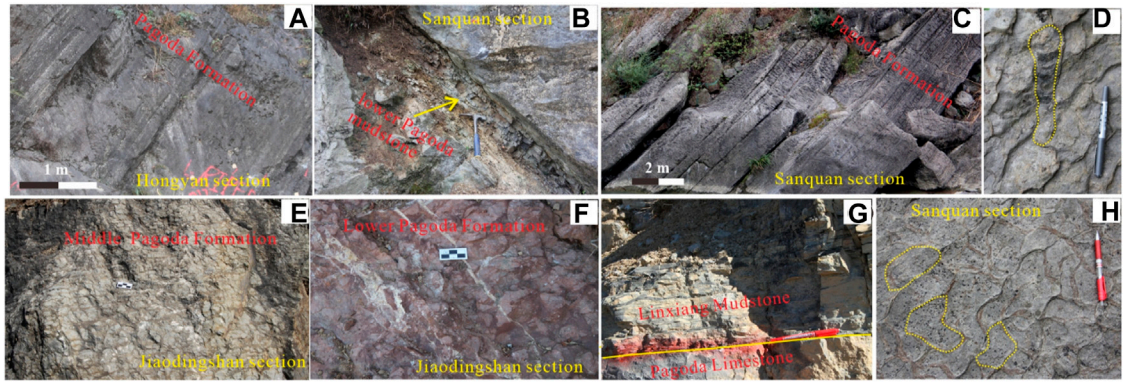

FIGURE 2
The outcrop photos of the study sections in the Upper Yangtze Platform. **(A)** The Pagoda Formation in the Hongyan section; **(B)** Lower Pagoda mudstone in the Sanquan section; **(C)** The Pagoda Formation in the Sanquan section; **(D)** The fossils in the Pagoda Formation of the Sanquan section; **(E)** The middle Pagoda limestone in the Jiaodingshan section; **(F)** The lower Pagoda Formation; **(G)** The contact of the Linxiang and Pagoda Formation; **(H)** The 'horse hoof crack' texture of the Pagoda limestone.

TABLE 1 The Ordovician stratigraphy division and the correlation at the Sichuan basin and the adjacent areas.

System	Series	Stage	Hongyan, Sichuan (Formation)	Liangcun, Guizhou (Formation)	Xiaogangwan, Chongqing (Formation)	Leibo, Sichuan (Formation)	Chenjiahe& Zhenjin,Hubei (Formation)	Jiaodingshan, Sichuan (Formation)
Upper Formation			Longmaxi	Longmaxi	Longmaxi	Longmaxi	Longmaxi	Longmaxi
Ordovician	Upper	Hirnantian	Wufeng	Wufeng	Wufeng	Wufeng	Wufeng	Wufeng
		Katian	Linxiang	Linxiang	Linxiang	Linxiang	Linxiang	Linxiang
		Sandbian	Pagoda	Pagoda	Pagoda	Pagoda	Pagoda	Pagoda
	Middle	Darriwilian	Miaopo	Shizipu	Guniutan	Qiaojia	Miaopo	Datianba
		Dapingian						

The yellow rectangle represents the studied areas.

where the Middle and Upper Ordovician were well exposed (Figures 2E, F), with the thickness of the study interval being 39.8 m. The Sanquan section is on the west of the riverside, northwest of Sanquan Town, Nanchuan District, Chongqing (29.14°N, 107.19°E). The study interval, which is 23.0 m, is a section discovered with three continuous and well-exposed Ordovician series (Figures 2B, C, D, G, H). The Hongyan section is a section situated in the south of Xikou Town, Huaying, Sichuan Province (30.16°N, 106.69°E), with the thickness of the study interval being 26.4 m (Figure 2A) (Ma et al., 2022).

The Upper Ordovician developed well in the Jiaodingshan section. It developed the Qiaojia, Pagoda, and Linxiang formations in ascending order (Table 1). The Lower Qiaojia Formation is made of purple-red mudstone that totals 7.8 m in thickness with 2.2 m of limestone developed at the top. The Pagoda Formation totals a thickness of 33.5 m including, from bottom to top, 8 m of purple-red limestone, 14.5 m of dark grey limestone, and 11 m of grey limestone. The Linxiang Formation is mainly formed of 3 m of dark grey mudstone and 2.5 m of grey limestone in ascending order. The partially covered black graptolite mudstone of the Longmaxi Formation can be seen on the upper outcrop.

In the Sanquan section, the Guniutan Formation (Table 1) is mainly composed of bioclastic limestone with a thickness of 17.3 m, with the *Baltoniodus variabilis* conodont zone being recognized on the top of this formation. The middle and lower Pagoda Formation is characterized by reddish and medium thick-bedded limestone, with grey mudstone about 30 cm thick at the bottom. The middle and upper Pagoda Formation is characterized by grey medium-thick bedded limestone with a thickness of 23.5 m, which is in parallel unconformity contact (paraconformity) with the underlying Guniutan Formation. It also yielded conodont fauna, and *Protopanderodus insculptus* and *Hamarodus brevirameus* zones were established in the Pagoda Formation. The Linxiang Formation is characterized by grey micritic limestone and nodular limestone, which is about 4 m thick. The Wufeng Formation (Table 1) is covered with black carbonaceous shale, calcareous mudstone, and marl, about 10 m thick, and produces a large number of graptolites.

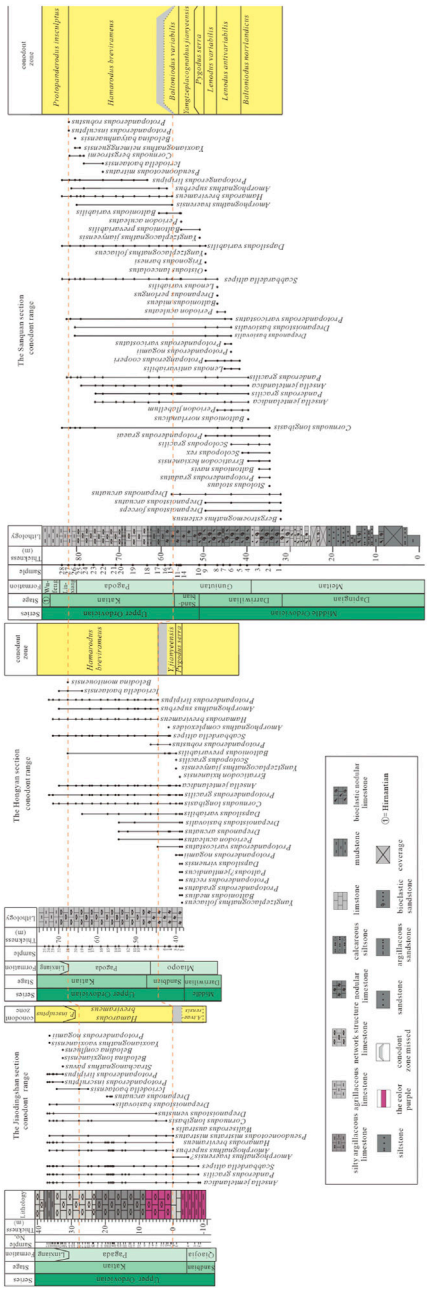

FIGURE 3
The conodont zone correlation among the Jiaodingshan, Hongyan, and Sanquan sections in the Sichuan Basin.

In the Hongyan section, the Miaopo Formation is constituted by grey limestone (9.5 m) with a 'horse hoof crack' texture, and the Pagoda Formation presents grey limestone (22.5 m). The Miaopo Formation is defined according to the occurrence of the conodont fauna, *Yangtzeplacognathus jianyeensis*. The *Y. jianyeensis* zone was widely established in the Ordovician Miaopo Formation of South China. The Miaopo Formation was also established in the Chenjiahe section of the Hubei province and is located near the Global Stratotype Section and Point for the Middle Ordovician Series.

The limestone of the Pagoda Formation is a large-scale and widely distributed strata in southern China. It has high consistency in the lithology in study sections, consisting of grey to light purplish red, middle-thick-bedded limestones with polygonal reticulate structure or 'horse hoof crack' texture that is especially apparent on bedding planes. Many scholars have studied its genesis, biological fossils, and duration (Sheng and Ji, 1984; An et al., 1985; Sheng and Ji, 1986; Mu et al., 1987; Ma et al., 2019b) and the results have significant implications for fossil fuels generation and paleoenvironment of the Yangtze Platform.

3 Materials and methods

3.1 Conodont fossil analytical method

In this study and search for conodonts, 28 samples were collected from the Qiaojia to the lower Linxiang Formation in the Jiaodingshan section. In total, 4, 21, and 3 samples were collected in the Qiaojia Formation, Pagoda Formation, and Linxiang Formation, respectively, with a weight of 5–7 kg per sample (Figure 3). The collected samples were broken into 2–3 cm^3 small pieces and digested in 10% acetic acid, and the insoluble substances at the bottom were separated every 2–3 days. The samples were screened to remove the residual acid and impurities with 20 mesh and 160 mesh sample sifters, respectively. After drying the screened samples, the conodonts were further separated by LST liquid with a density of 2.80 g/mL. At last, abundant conodonts were obtained under binocular stereography.

3.2 Carbon and oxygen isotope analytical method

In order to carry out the carbon and oxygen isotope stratigraphic analysis, 61 samples were obtained from the Qiaojia to Linxiang Formation of the Jiaodingshan section. In all, 42 samples were obtained from the Sanquan section and 53 samples were obtained from the Hongyan section. The samples were carefully selected in the Palaeontology Laboratory of the Research Institute of the Petroleum Exploration and Development, PetroChina, and ground into 200 g of powder using a micro-drill, avoiding the samples from becoming polluted. The samples were first ground before a mm-sized hole was drilled. Then the samples were processed in the Isotope Laboratory of the Nanjing Institute of Geology and Palaeontology, CSA. The powder was reacted with 100% anhydrous phosphoric acid for 24 h at 22°C± 1°C and 50% RH± 5% in humidity to produce CO_2. The samples were then tested on the Thermo Scientific MAT 253 stable isotope mass spectrometer. The standard isotope sample is GBW-04405 (National Standard) ($\delta^{13}C$= 0.57, $\delta^{18}O$= −8.49). The analysis results of $\delta^{13}C$ and $\delta^{18}O$ (both Vienna Pee Dee Belemnite values) were obtained with 0.03 and 0.14 standard deviations, respectively (Table 2).

4 Results

4.1 Conodont biostratigraphy

Three conodont zones were established in ascending order based on the conodont fauna collected from the Jiaodingshan and Hongyan sections, respectively.

10.3389/feart.2023.1220173

TABLE 2 The carbon and oxygen isotope data and the scatter diagrams from the Middle-Upper Ordovician in the Sanquan, Hongyan, and Jiaodingshan sections.

No.	δ13C(‰)	δ18O(‰)	Meters (m)	Formation	
Sanquan section					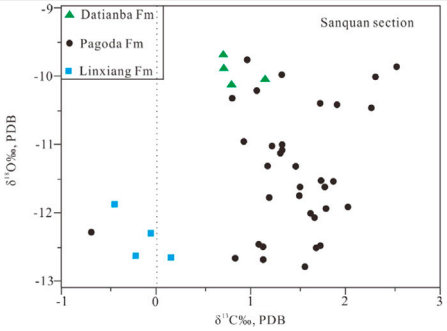
SQ-T-1	−0.1	−12.3	2.0	Linxiang	
SQ-T-2	−0.4	−11.9	2.4	Linxiang	
SQ-T-3	−0.2	−12.7	2.8	Linxiang	
SQ-T-4	0.1	−12.7	3.2	Linxiang	
SQ-T-5	0.8	−12.7	3.8	Pagoda	
SQ-T-6	1.1	−12.7	4.8	Pagoda	
SQ-T-7	1.1	−12.5	5.3	Pagoda	
SQ-T-8	1.1	−12.5	6.1	Pagoda	
SQ-T-9	1.7	−12.5	6.9	Pagoda	
SQ-T-10	1.7	−12.6	7.3	Pagoda	
SQ-T-11	1.6	−12.1	8.3	Pagoda	
SQ-T-12	2	−12	9.1	Pagoda	
SQ-T-13	1.8	−12	9.9	Pagoda	
SQ-T-14	1.2	−11.8	10.9	Pagoda	
SQ-T-15	1.7	−11.6	11.7	Pagoda	
SQ-T-16	1.7	−12.1	12.4	Pagoda	
SQ-T-17	1.5	−11.8	13.5	Pagoda	
SQ-T-18	1.5	−11.7	14.5	Pagoda	
SQ-T-19	1.8	−11.7	15.5	Pagoda	
SQ-T-20	−0.7	−12.3	15.9	Pagoda	
SQ-T-21	1.9	−11.6	16.4	Pagoda	
SQ-T-22	1.6	−12.8	17.4	Pagoda	
SQ-T-23	1.2	−11.3	18.7	Pagoda	
SQ-T-24	1.3	−11.2	19.8	Pagoda	
SQ-T-25	0.9	−11	20.5	Pagoda	
SQ-T-26	1.3	−11.1	21.5	Pagoda	

(Continued on following page)

TABLE 2 (*Continued*) The carbon and oxygen isotope data and the scatter diagrams from the Middle-Upper Ordovician in the Sanquan, Hongyan, and Jiaodingshan sections.

No.	δ13C(‰)	δ18O(‰)	Meters (m)	Formation	
SQ-T-27	1.2	−11.1	21.9	Pagoda	
SQ-T-28	1.3	−11	23.0	Pagoda	
SQ-T-29	1.5	−11.4	23.5	Pagoda	
SQ-T-30	1.9	−10.4	24.5	Pagoda	
SQ-T-31	1.7	−10.4	25.5	Pagoda	
SQ-T-32	2.3	−10.4	26.6	Pagoda	
SQ-T-33	2.5	−9.9	27.7	Pagoda	
SQ-T-34	2.3	−10	28.7	Pagoda	
SQ-T-35	1.3	−10	29.5	Pagoda	
SQ-T-36	1.1	−10.2	30.2	Pagoda	
SQ-T-37	0.8	−10.4	31.1	Pagoda	
SQ-T-38	1	−9.8	31.9	Pagoda	
SQ-T-39	0.7	−9.9	33.0	Datianba	
SQ-T-40	0.7	−9.7	33.6	Datianba	
SQ-T-41	0.8	−10.1	33.9	Datianba	
SQ-T-42	1.1	−10	35.3	Datianba	
Hongyan section					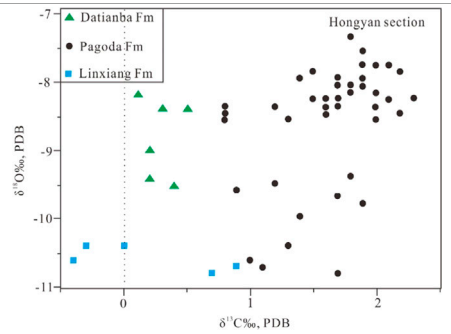
HY-T-1	−0.4	−10.6	71.5	Linxiang	
HY-T-2	−0.3	−10.4	71	Linxiang	
HY-T-3	0	−10.4	70.5	Linxiang	
HY-T-4	0.7	−10.8	70	Linxiang	
HY-T-5	0.9	−10.7	69.5	Linxiang	
HY-T-6	1	−10.6	69	Pagoda	
HY-T-7	1.1	−10.7	68.5	Pagoda	
HY-T-8	1.7	−10.8	68	Pagoda	
HY-T-9	1.9	−9.8	67.5	Pagoda	
HY-T-10	1.3	−10.4	67	Pagoda	

(Continued on following page)

10.3389/feart.2023.1220173

10.3389/feart.2023.1220173

TABLE 2 (*Continued*) The carbon and oxygen isotope data and the scatter diagrams from the Middle-Upper Ordovician in the Sanquan, Hongyan, and Jiaodingshan sections.

No.	δ13C(‰)	δ18O(‰)	Meters (m)	Formation	
HY-T-11	1.4	−10	66.5	Pagoda	
HY-T-12	1.7	−9.7	66	Pagoda	
HY-T-13	1.2	−9.5	65.5	Pagoda	
HY-T-14	1.8	−9.4	65	Pagoda	
HY-T-15	2	−8.6	64.5	Pagoda	
HY-T-16	1.7	−8.4	64	Pagoda	
HY-T-17	2.2	−8.5	63.5	Pagoda	
HY-T-18	2.1	−8.3	63	Pagoda	
HY-T-19	2.3	−8.3	62.5	Pagoda	
HY-T-20	2	−8.4	62	Pagoda	
HY-T-21	1.9	−7.6	61.5	Pagoda	
HY-T-22	1.9	−7.8	61	Pagoda	
HY-T-23	1.9	−8.1	60.5	Pagoda	
HY-T-24	2	−7.8	60	Pagoda	
HY-T-25	1.8	−7.4	59.5	Pagoda	
HY-T-26	1.9	−8.1	59	Pagoda	
HY-T-27	2	−8.2	58.5	Pagoda	
HY-T-28	1.9	−8	58	Pagoda	
HY-T-29	1.8	−8.1	57.5	Pagoda	
HY-T-30	1.8	−8.2	57	Pagoda	
HY-T-31	1.7	−8	56.5	Pagoda	
HY-T-32	1.7	−8.1	56	Pagoda	
HY-T-33	2.2	−7.9	55.5	Pagoda	
HY-T-34	2.1	−7.8	55	Pagoda	
HY-T-35	1.6	−8.5	54.5	Pagoda	
HY-T-36	1.7	−8.3	54	Pagoda	
HY-T-37	1.5	−7.9	53.5	Pagoda	

(Continued on following page)

TABLE 2 (*Continued*) The carbon and oxygen isotope data and the scatter diagrams from the Middle-Upper Ordovician in the Sanquan, Hongyan, and Jiaodingshan sections.

No.	δ13C(‰)	δ18O(‰)	Meters (m)	Formation	
HY-T-38	1.4	−8	53	Pagoda	
HY-T-39	1.3	−8.6	52.5	Pagoda	
HY-T-40	1.6	−8.3	52	Pagoda	
HY-T-41	1.6	−8.4	51.5	Pagoda	
HY-T-42	1.5	−8.3	51	Pagoda	
HY-T-43	1.2	−8.4	50.5	Pagoda	
HY-T-44	0.8	−8.4	50	Pagoda	
HY-T-45	0.9	−9.6	49.5	Pagoda	
HY-T-46	0.8	−8.5	49	Pagoda	
HY-T-47	0.8	−8.6	48.5	Pagoda	
HY-T-48	0.2	−9.4	48	Datianba	
HY-T-49	0.5	−8.4	47.5	Datianba	
HY-T-50	0.1	−8.2	47	Datianba	
HY-T-51	0.4	−9.5	46.5	Datianba	
HY-T-52	0.2	−9	46	Datianba	
HY-T-53	0.3	−8.4	45.5	Datianba	
Jiaodingshan section					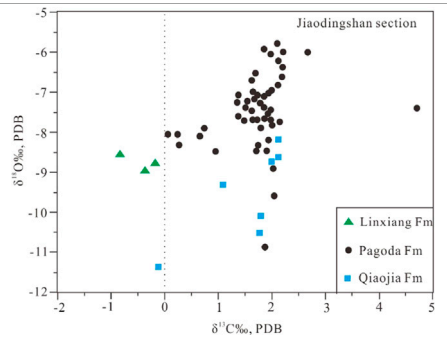
JDS-T-61	−0.4	−8.9	47.5	Linxiang	
JDS-T-60	−0.2	−8.7	47	Linxiang	
JDS-T-59	−0.8	−8.5	46.5	Linxiang	
JDS-T-58	0.7	−8.1	46	Pagoda	
JDS-T-57	0.3	−8.3	45.7	Pagoda	
JDS-T-56	0.3	−8.1	45.4	Pagoda	
JDS-T-55	0.1	−8.1	45	Pagoda	
JDS-T-54	0.8	−7.9	44.5	Pagoda	
JDS-T-53	1.4	−7.6	44.2	Pagoda	
JDS-T-52	1.4	−7.3	44	Pagoda	

(Continued on following page)

10.3389/feart.2023.1220173

TABLE 2 (*Continued*) The carbon and oxygen isotope data and the scatter diagrams from the Middle-Upper Ordovician in the Sanquan, Hongyan, and Jiaodingshan sections.

No.	δ13C(‰)	δ18O(‰)	Meters (m)	Formation	
JDS-T-51	2.1	−6.3	43.5	Pagoda	
JDS-T-50	2.1	−6.8	43.1	Pagoda	
JDS-T-49	2	−7	43	Pagoda	
JDS-T-48	1	−8.5	42.5	Pagoda	
JDS-T-47	1.5	−7.7	42	Pagoda	
JDS-T-46	1.8	−8.4	41	Pagoda	
JDS-T-45	1.8	−7.9	40	Pagoda	
JDS-T-44	2.6	−6	39.5	Pagoda	
JDS-T-43	1.9	−7.5	38.5	Pagoda	
JDS-T-42	1.6	−7.4	38	Pagoda	
JDS-T-41	2	−6.1	37	Pagoda	
JDS-T-40	2.1	−5.8	36.15	Pagoda	
JDS-T-39	1.7	−7.7	35.4	Pagoda	
JDS-T-38	1.9	−7.4	35	Pagoda	
JDS-T-37	1.9	−7.6	34	Pagoda	
JDS-T-36	2	−7.5	33.7	Pagoda	
JDS-T-35	1.81	−7.3	32.5	Pagoda	
JDS-T-34	1.6	−7.2	31.2	Pagoda	
JDS-T-33	1.4	−7.1	30	Pagoda	
JDS-T-32	1.9	−6	29.6	Pagoda	
JDS-T-31	1.9	−8.5	29.3	Pagoda	
JDS-T-30	2.2	−6.7	29	Pagoda	
JDS-T-29	2.1	−7.7	28.5	Pagoda	
JDS-T-28	2	−9.6	28	Pagoda	
JDS-T-27	2.2	−6	27.7	Pagoda	
JDS-T-26	2.2	−6.4	27.4	Pagoda	
JDS-T-25	2	−8.9	26.4	Pagoda	

(Continued on following page)

10.3389/feart.2023.1220173

10.3389/feart.2023.1220173

TABLE 2 (*Continued*) The carbon and oxygen isotope data and the scatter diagrams from the Middle-Upper Ordovician in the Sanquan, Hongyan, and Jiaodingshan sections.

No.	δ13C(‰)	δ18O(‰)	Meters (m)	Formation	
JDS-T-24	2	−7.8	25.8	Pagoda	
JDS-T-23	1.9	−8.2	24.75	Pagoda	
JDS-T-22	1.9	−10.9	24.2	Pagoda	
JDS-T-21	2	−7.1	23	Pagoda	
JDS-T-20	2	−7.7	22.7	Pagoda	
JDS-T-19	1.7	−7.1	21.5	Pagoda	
JDS-T-18	1.7	−7.7	20.3	Pagoda	
JDS-T-17	1.9	−7.1	19.75	Pagoda	
JDS-T-16	1.6	−7.5	18.5	Pagoda	
JDS-T-15	1.7	−7	17	Pagoda	
JDS-T-14	1.7	−6.7	16	Pagoda	
JDS-T-13	1.7	−6.6	15	Pagoda	
JDS-T-12	1.7	−6.6	13.5	Pagoda	
JDS-T-11	1.7	−7.2	12.85	Pagoda	
JDS-T-10	1.7	−8.5	12	Pagoda	
JDS-T-9	1.9	−7.7	11.5	Pagoda	
JDS-T-8	4.7	−7.4	10.8	Pagoda	
JDS-T-7	2.1	−8.2	10.5	Qiaojia	
JDS-T-6	2	−8.7	10	Qiaojia	
JDS-T-5	2.1	−8.6	9	Qiaojia	
JDS-T-4	1.8	−10.1	5.5	Qiaojia	
JDS-T-3	−0.1	−11.4	3.5	Qiaojia	
JDS-T-2	1.8	−10.6	2.5	Qiaojia	
JDS-T-1	1.1	−9.3	2	Qiaojia	

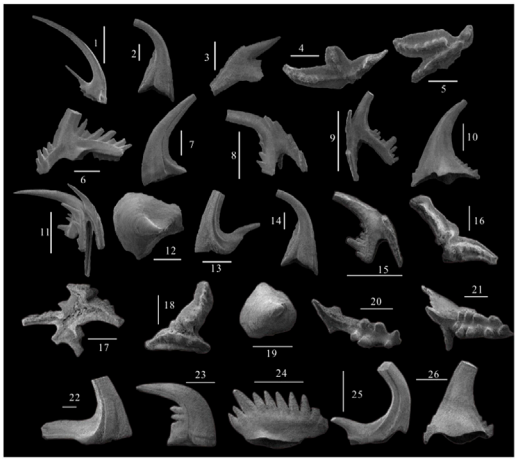

FIGURE 4
The Late Ordovician conodonts in the Jiaodingshan, Hongyan, and Sanquan sections of the Sichuan Basin. The scale bar corresponds to 200 μm. (**1**) *Erraticodon hexianensis*, lateral view, sample SQN-Y-1; (**2**) *Scabbardella altipes*, lateral view, sample SQN-Y-22; (**3**) *Baltoniodus medius*, lateral view, sample SQN-Y-9; (**4**) *Yangtzeplacognathus foliaceus*, lateral view, sample SQN-Y-9; (**5**) *Yangtzeplacognathus jianyeensis*, lateral view, sample SQN-Y-10; (**6**) *Periodon aculeatus*, lateral view, sample SQN-Y-9; (**7**) *Dapsilodus variabilis*, lateral view, sample SQN-Y-25; (**8**) *Baltoniodus variabilis*, lateral view, sample SQN-Y-12; (**9**) *Hamarodus brevirameus*, lateral view, sample SQN-Y-13; (**10**) *Hamarodus brevirameus*, lateral view, sample SQN-Y-20; (**11**) *Amorphognathus superbus*, bottom view, sample SQN-Y-16; (**12**) *Pseudooneotodus mitratus*, bottom view, sample SQN-Y-20; (**13**) *Protopanderodus insculptus*, lateral view, sample SQN-Y-27; (**14**) *Scabbardella altipes*, lateral view, sample SQN-Y-22; (**15**) *Amorphognathus tvaerensis*, lateral view, sample 16-004; (**16**) *Amorphognathus superbus*, lateral view, sample 16-006; (**17**) *Amorphognathus superbus*, aboral view, sample 16-009; (**18**) *Amorphognathus superbus*, oral view, sample 16-0012; (**19**) *Pseudooneotodus mitratus*, oral view, sample 16-007; (**20**) *Icriodella baotaensis*, oral view, sample 16-0022; (**21**) *Icriodella baotaensis*, oral view, sample 16-0025; (**22**) *Protopanderodus liripipus*, lateral view, sample 16-0028; (**23**) *Belodina longxianensis*, lateral view, sample 16-0026; (**24**) *Yaoxianognathus yaoxianensis*, lateral view, sample 17-0010; (**25**) *Protopanderodus insculptus*, lateral view, sample 16-0029; (**26**) *Hamarodus brevirameus*, lateral view, sample 17-008.

4.1.1 Jiaodingshan section

4.1.1.1 *Amorphognathus tvaerensis* Zone

The *Amorphognathus tvaerensis* conodont zone was established in the lower Pagoda Formation and upper Qiaojia Formation. The base of this zone was the first appearance datum (FAD) of *A. tvaerensis* [Figure 4 (15)] and its top could not be defined because the conodont fauna was rare. Other conodonts include *Ansella jemtelandica* (Löfgren, 1978)[1], *Scabbardella altipes* (Henningsmoen, 1948)[1], *P. gracilis* (Branson et Mehl, 1933)[1], *Baltoniodus* sp., *Triangulodus* sp., and *Drepanoistodus* sp.

4.1.1.2 *Hamarodus brevirameus* Zone

The *H. brevirameus* conodont zone was established in the middle-lower Pagoda Formation. The base of this zone was the FAD of *H. brevirameus* and its top was the FAD of *P. insculptus*. Other conodonts included *Amorphognathus superbus* (Rhodes, 1953)[1] [Figures 4 (16–18)], *Pseudooneotodus mistratus* (Moskalenko, 1973)[1] [Figures 4 (12,19)], *Icriodella baotaensis* (An, Du, Gao, Chen et lee, 1981)[1] [Figures 4 (20,21)], *S. altipes* (Henningsmoen, 1948)[1], *Panderodus gracilis* (Branson et Mehl, 1933)[1], *Drepanoistodus venustus* (Stauffer 1935)[1], *D. basiovalis* (Sergeeva, 1963)[1], *Drepanodus arcuatus* (Pander, 1856)[1], *C. longibasis* (Lingström, 1955)[1], and *Walliserodus australis* (Serpaglis, 1974)[1].

4.1.1.3 *Protopanderodus insculptus* Zone

The *P. insculptus* conodont zone was established in the upper Pagoda and Linxiang Formation. The base of this zone was the FAD of *P. insculptus* and its top could not be defined because the conodont fauna was scarce. Other conodonts fauna were commensal with the *P. insculptus* including *Protopanderodus liripipus* [Figure 4 (22)] (Kennedy, Barnes et Uyeno, 1979)[1], *H. brevirameus* (Serpagli, 1964)[1], *Belodina longxianensis* [Figure 4 (23)] (Wang et al., 1984)[1], *Belodina confluens* (Sweet, 1979)[1], *Strachanognathus pavus* (Rhodes, 1955)[1], *Ansella jemtelandic* (Löfgren, 1978)[1], *S. altipes* (Henningsmoen, 1948)[1], *Panderodus gracilis* (Branson et Mehl, 1933)[1], *P. mistratus* (Moskalenko, 1973)[1], *I. baotaensis* (An, Du, Gao, Chen et lee, 1981)[1], *D. venustus* (Stauffer 1935)[1], and *Drepanoistodus basiovalis* (Sergeeva, 1963)[1].

4.1.2 Hongyan section

4.1.2.1 *Pygodus serra* Zone (*Yangtzeplacognathus foliaceus* subzone)

The *Pygodus serra* conodont zone was established in the upper Datianba Formation. The base of this zone was the FAD of *Yangtzeplacognathus foliaceus* (Fahraeus, 1966)[1] and its top was the FAD of *Y. jianyeensis* (*Pygodus anserinus*). Other conodont faunas were commensal with the *Y. foliaceus* including *Baltoniodus medius* (Dzik, 1976)[1], *Erraticodon hexianensis* (An et al., 1985), *Periodon aculeatus* (Hadding, 1913)[1], *A. jemtelandica* (Löfgren, 1978)[1], *Protopanderodus varicostatus* (Sweet et Bergström, 1962)[1], *Protopanderodus gradatus* (Serpagli, 1974)[1], *Protopanderodus rectus* (Lindström, 1955)[1], *Protopanderodus nogamii* (Lee, 1975)[1], *P. gracilis* (Branson et Mehl, 1933)[1], *C. longibasis* (Lingström, 1955)[1], *D. arcuatus* (Pander, 1856)[1], and *D. basiovalis* (Sergeeva, 1963)[1].

4.1.2.2 *Yangtzeplacognathus jianyeensis* Zone

The *Y. jianyeensis* conodont zone was established in the Miaopo Formation. The base of this zone was the FAD of *Y. jianyeensis* (An et Ding, 1982)[1] and its top could not be defined because the conodont fauna was rare. Other conodont fauna was commensal with the *Y. jianyeensis* including *S. altipes* (Henningsmoen, 1948)[1], *Baltoniodus prevariabilis* (Fahraeus, 1966)[1], *Amorphognathus complexoides* (An, 1987), *P. nogamii* (Lee, 1975)[1], *Protopanderodus robustus* (Hadding, 1913)[1], *Dapsilodus variabilis* (Webers, 1964)[1], *A. jemtelandica* (Löfgren, 1978)[1], *P. gracilis* (Branson et Mehl, 1933)[1], *C. longibasis* (Lingström, 1955)[1], and *D. arcuatus* (Pander, 1856)[1].

4.1.2.3 *Hamarodus brevirameus* Zone

Hamarodus brevirameus conodont zone was established in the lower Pagoda Formation. The base of this zone was the FAD of *H. brevirameus* and its top could not be defined because the conodonts were rare. Other conodont faunas were commensal

1 Next to the conodont fauna names in the text are listed the names of the individuals who were first considered in the field to have identified the specie of the conodont.

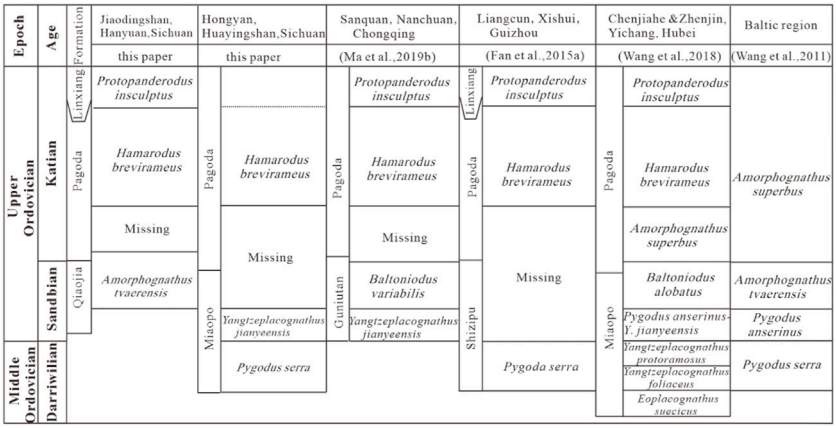

FIGURE 5
Middle-Upper Ordovician conodont zonation correlation in the Baltic region and Yangtze Platform.

with the *H. brevirameus* including *A. superbus* (Rhodes, 1953)[1], *Protopangerodus liripipus* (Kennedy, Barnes et Uyeno, 1979)[1], *Belodina monitouensis* (Ethington et Schumacher, 1969)[1], *I. baotaensis* (An, Du, Gao, Chen et Lee, 1981)[1], and *P. mistratus* (Moskalenko, 1973)[1].

4.1.3 Conodont Zones correlation

The conodont zonation established in the Jiaodingshan and Hongyan sections is introduced and discussed in ascending order as follows.

4.1.3.1 *Pygodus serra* Zone (*Yangtzeplacognathus foliaceus* subzone)

The lower part of the zone of *P. serra* was established in the Guniutan Formation of the upper Darriwilian in Tangshan, Nanjing (An, 1987; Wang, 1993; Wang et al., 2011) and the Guniutan Formation in Xishui, Guizhou (Fan et al., 2015a). Thus, the zone of *P. serra*, established in the two study sections, correlated well with the zone of *P. serra* established in the two areas mentioned above. Moreover, the *P. serra* zone could correlate with the *P. serra* zone of the Darriwilian strata of the Baltic region (Figure 5). In addition, the *Yangtzeplacognathus protoramosus* and *Y. foliaceus* zones established in the Miaopo Formation and exposed in the Huanghuachang and Chenjiahe section in Yichang, Hubei, were subzones of the *P. serra* zone that could correlate with part of the *P. serra* zone defined in the Hongyan section. The zonation of conodonts was continuous in the two sections of Yichang, Hubei.

4.1.3.2 *Yangtzeplacognathus jianyeensis* Zone

According to the definition and evolution of this biozone in China, *Y. jianyeensis* zone, *P. anserinus* zone, and *Y. jianyeensis-P. anserinus* zones all refer to one same conodont biozone because experts illustrate that due to different lithofacies and areas, different conodont species could exist in the same strata (An et al., 1981; Wang et al., 2017). The *Y. jianyeensis-P. anserinus* zone was established in the Katian and Miaopo Formation in the Huanghuachang, Yichang, Hubei (An et al., 1985). The *Y. jianyeensis* zone was recognized in the Sandbian and Guniutan formations in the Sanquan, Nanchuan, and Chongqing. So, the *Y. jianyeensis* zone established in the studied Hongyan section could be correlated with the two conodont biozones mentioned above. In addition, it could also correlate with the *P. anserinus* zone established in the Katian strata in the Baltic region (Figure 5). The *P. anserinus-Y. jianyeensis*, *Baltoniodus alobatus*, *A. superbus*, *H. brevirameus*, and *P. insculptus* zones were established from the Sandbian to Katian strata in the Chenjiahe and Zhenjin section of the Yichang, Hubei, in ascending order. Correlating with the continuous zonation in the Yichang area, the *B. alobatus* and *A. superbus* zones were missing in the Hongyan section. The *Y. jianyeensis* zone could not be established in the Jiaodingshan section due to the absence of biostratigraphically significant taxa.

4.1.3.3 *Amorphognathus tvaerensis* Zone

This biozone was initially established in the Datianba Formation of Nanjing, Jiangsu (same as Miaopo and Qiaojia Formation) (Wang, 1993). The biozone was also established in the Sandbian from the Baltic region (Bergström, 1982). So, the *A. tvaerensis* zone built in the Jiaodingshan could be correlated with the same name conodont biozone mentioned above. The *B. alobatus* and *B. variabilis* zones in the Chenjiahe and Sanquan sections are subzones of the *A. tvaerensis* zone that can correlate with part of the *A. tvaerensis* zone (Wang et al., 2013)[1]. The continuous conodont zonation from the Sandbian to Katian in age from the Chenjiahe and Zhenjin section of the Yichang area are, in ascending order: *P. anserinus-Y. jianyeensis*, *B. alobatus*, *A. superbus*, *H. brevirameus*, and *P. insculptus* zones. Correlating with the continuous zonation in the Yichang area, the *A. superbus* zone was missing in the Jiaodingshan section (Figure 5).

4.1.3.4 *Hamarodus brevirameus* Zone

This biozone exists in the middle portion of the Pagoda Formation in South China (An, 1987; et al., 2011) and was recognized in the Pagoda Formation in Nanchuan, Chongqing (Ma et al., 2019b), in Xishui, Guizhou, and Yichang, Hubei. So, the *H. brevirameus* zone built in the Jiaodingshan and Hongyan sections could be correlated with the same name conodont biozone mentioned above (Figure 5). The *H. brevirameus* zone could also

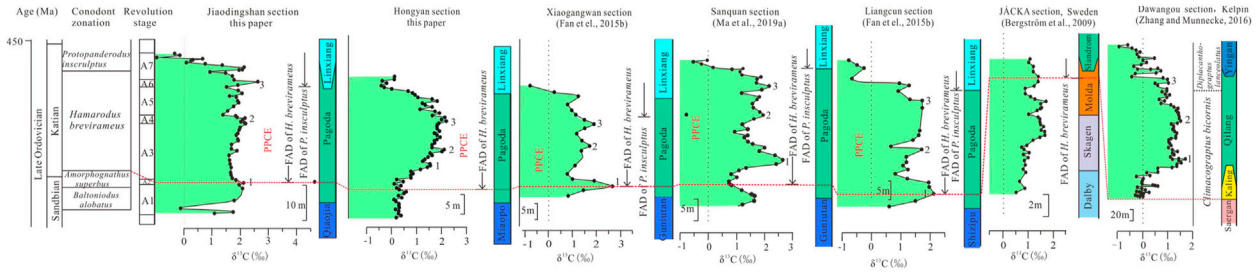

FIGURE 6
$\delta^{13}C$ isotope correlation in Middle-Upper Ordovician of the Sichuan Basin, Kelpin area, Xinjiang, and Sweden.

correlate with the upper portion of the *A. superbus* zone subdivided in the Baltic region, which is Katian in age (Bergström, 1982; Ding et al., 1993).

4.1.3.5 *Protopanderodus insculptus* Zone

This conodont biozone exists in the Upper Ordovician Pagoda and Linxiang Formation of South China (An, 1987; Wang et al., 2011). It was established in the Upper Ordovician Pagoda and Linxiang Formation in the Nanchuan, Chongqing (Ma et al., 2019b), Xishui, Guizhou (Fan et al., 2015a), and Huanghuachang and Zhenjin, Yichang, Hubei (Wang Z. H. et al., 2018). So, the *P. insculptus* zone established in the Jiaodingshan section could be correlated with the same name biozone mentioned above (Figure 5), and no *P. insculptus* element was found in the sample collected from the Hongyan section.

Compared with the continuous conodont zonation in the Yichang and Baltic regions, one to three conodont bizones were missing in the two study sections and adjacent areas in the Upper Yangtze Platform through the Katian to the Sandbian strata. The *A. superbus* zone was missing in the strata of the Jiaodingshan section. The *A. superbus* and *A. tvaerensis* zones were missing in the strata of the Hongyan section. The *A. superbus* zone was missing in the strata of the Sanquan section and the *A. superbus*, *A. Tvaerensis,* and *Y. jianyeensis* zones were missing in the strata exposed in the Liangcun section.

4.2 Characteristics and evolutionary trend of $\delta^{13}C$ isotope composition

The $\delta^{13}C$ isotope samples analyzed were collected in the Qiaojia, Pagoda, and Linxiang Formations. According to the characteristics of lithology and isotopic value, the Upper Ordovician in the Jiaodingshan section was divided into seven isotopic stages from the bottom to the top, respectively, named A1 to A7 (Figure 6). The A1 and A2 could be correlated with the Upper Qiaojia Formation and the bottom of the Pagoda Formation. A3–A6 and lower A7 correlated with the Pagoda Formation. The middle and upper A7 stages were defined in the Lower Linxiang Formation.

4.2.1 Upper Qiaojia Formation

The characteristics of the carbon isotope curve obtained from the samples of the upper part of the Qiaojia Formation are as follows (Figure 6): At stage A1, the $\delta^{13}C$ value decreased from 1.1‰ to −0.1‰, and then rose to 2.0‰, reaching stage A2, where there was a peak value of 2.1‰, including an abnormally high value of 4.7‰ deleted in the figure, which may indicate that the latter value could be affected by the late diagenetic transformation.

4.2.2 Pagoda Formation

The $\delta^{13}C$ values of the Pagoda Formation were all positive, and the middle and lower parts of the Pagoda Formation included the A3 stage with a small variation range of 1.6‰–2.0‰. There were two positive peaks in the middle and upper part of the Pagoda Formation. The first peak of 2.2‰ was in the middle part of the Pagoda Formation, which was stage A4, after which the $\delta^{13}C$ value dropped to 1.4‰. After a small range of fluctuations, it reached the next peak of 2.6‰, which was related to stage A6. The middle stage was A5, where the variation range of $\delta^{13}C$ value was approximately 0.6‰.

5 Discussion on the contact relationship between the Pagoda Formation and the underlying formation

5.1 Reliability of the isotopic data

In order to ensure the validity of carbon and oxygen isotope data, fresh rocks without veins and fractures were selected for sample collection in the rock outcrop, and the structure of late striking, recrystallization, and pore fracture were avoided as far as possible. The fresh rock samples were ground indoors, and the quality was guaranteed by avoiding the calcite vein. First, the validity of the carbon isotope data was analyzed based on oxygen isotope data. The accepted range of the effective $\delta^{18}O$ was greater than −10‰ (Kaufman and Knoll, 1995; Zhu et al., 2004; Li et al., 2009), and the results demonstrated that almost all the $\delta^{18}O$ values obtained in the Jiaodingshan section were greater than −10‰. However, a $\delta^{18}O$ value of less than −10‰ carbon isotope value is not fully determined to be invalid data because of the following reasons. Small amounts of carbon are exposed to carbonate rocks based on the low carbon concentration of diagenetic pore fluid. The atmospheric freshwater or hydrothermal water, which promotes the oxygen isotope rebalancing, sometimes is not strong enough to

change the value of the carbon isotope, so the carbon isotope is less easily affected by the diagenesis compared with the oxygen isotope (Anderson and Arthur, 1983; Glumac and Spivak-Birndord, 2002). Hence, in the actual study, even if the value of $\delta^{18}O$ is less than −10‰, the value of $\delta^{13}C$ may still be valid (Dilliard, 2007; Wotte et al., 2007)[1]. Therefore, although the negative value of $\delta^{18}O$ of a sample could be used as a good index to determine whether the value of $\delta^{18}O$ is affected by the diagenetic, how it effectively indicates the change of carbon isotope composition needs to be further studied and should be used in combination with other methods (Dilliard, 2007; Wotte et al., 2007)[1].

The second method to ensure the validity of carbon isotope data is the scatter plot of the $\delta^{13}C$ and $\delta^{18}O$ (Table 2). There is no linear correlation between the two data series, showing a dispersed distribution. This indicates that the strata were not deposited under the influence of diagenetic transformation (Bathurst, 1972; Brand and Veizer, 1980; Brasier et al., 1990; Brasier et al., 1996; Dilliard, 2007). All in all, combining these two methods, the $\delta^{13}C$ and $\delta^{18}O$ values in the study sections were considered to be reliable (Table 2). The isotopic results in the Sanquan and Hongyan sections are quoted from Ma et al. (2019c), Ma et al. (2022).

5.2 The top of the Pagoda Formation and Linxiang Formation

In the isotopic seven stages, there were three distinct positive excursions of $\delta^{13}C$ values in the range of 2.0‰–3.0‰ in A2, A4, and A6, with the first lower peak occurring at the first appearance of conodont *H. brevirameus*. This positive excursion of $\delta^{13}C$ isotopes was found not only in the Jiaodingshan area but also in the Xiaogangwan (Qixian, Chongqing) and Sanquan (Nanchuan, Chongqing) areas, both located in the eastern Upper Yangtze Platform, the Liangcun area, located in the southern part of the Upper Yangtze Platform, the Hongyan area, and even in the Dawangou section, which is the Late Ordovician GSSP (Global boundary Stratotype Section and Point), in the Kelpin area and is located in the western margin of the Tarim Basin (Hennissen et al., 2016).

Some authors interpreted this event as a global carbon isotope excursion event, Guttenberg $\delta^{13}C$ Excursion (GICE) (Bergström et al., 2009). However, we compared it with the strata developing conodont fossils of North America (Bergström and Ferretti, 2017; MacDonald et al., 2017) and defined this positive excursion event as PPCE (Pagoda Positive $\delta^{13}C$ Excursion), which occurred in a higher layer than the layer occurring in the GICE event. It is believed that it is not the GICE event, but a new carbon isotope positive event, PPCE, represented at least regionally. PPCE developed in the Middle-Late Katian and Late Ordovician, while the Guttenberg $\delta^{13}C$ Excursion (GICE) defined in the Baltoscandia and America, extended from the Late Sandbian to the Early Katian. Moreover, it was demonstrated that the PPCE (3.68–4.37 myr) and GICE (2.35 myr) events have different durations based on cyclostratigraphic results by Ma et al. (2022). The unconformity most likely results in different durations of the PPCE. The main difference of the PPCE in different sections is one of the three secondary positive excursions (P1) occurring in the early period of the event. The P1 recognized in the Pagoda Formation is less completed in the Hongyan section than in the Sanquan section, which illustrates that the Pagoda Formation is in parallel unconformity contact with the underlying strata and the stratigraphic gap underlying the Pagoda Formation in the Sanquan section is larger than that in the Hongyan section. The comparison results and the duration time have been published in another study and will not be discussed in-depth (Ma et al., 2022).

5.3 Defining the chemostratigraphic and stratigraphic gap underlying the Pagoda Formation

It has been found that there are several regions in the Upper Yangtze Platform with very similar carbon isotope characteristics and similar sedimentary backgrounds, all of which are found in the Pagoda Formation. The Pagoda Formation is the most widely distributed and easily recognized early Paleozoic strata in the Yangtze Platform. The lithologic characteristic is grey or light purplish argillaceous limestone, with a “horse hoof crack” texture. A large number of conodont faunas were found there. The study of carbon isotope characteristics and conodont zones in different areas of the Yangtze Platform is instructive for studying the development of the Pagoda Formation and estimating the missing amount of the underlying strata. The Xiaogangwan section (Qixian, Chongqing province) and Sanquan section (Nanchuan, Chongqing province), located in the eastern Upper Yangtze Platform, the Liangcun section (Xishui, Guizhou province), located in the southern portion, and the Jiaodingshan section, located in the western portion, were chosen to discuss the hiatus underlying the Pagoda Formation.

The characteristics of the $\delta^{13}C$ isotope curve in the strata of the studied Jiaodingshan section could be correlated with the Xiaogangwan section and the adjacent Sanquan section (Fan et al., 2015b; Ma et al., 2019a) (Figure 6). Comparing the two profiles, the Middle and Upper Ordovician carbon isotopic assemblages in the Jiaodingshan section were composed of three positive secondary excursions, with peak values ranging from 2.0‰ to 3.0‰. All of them began to develop at the bottom of the Pagoda Formation and extended upward to the middle and upper Pagoda Formation. The positive excursion events all began at the first appearance of the conodont *H. brevirameus*, and the largest peak in the Jiaodingshan section belongs to the upper Pagoda Formation, while the largest peaks in the Xiaogangwan and Sanquan sections belong to the lower Pagoda Formation. Regarding the $\delta^{13}C$ isotope sequence at the bottom of the Pagoda Formation, it was observed that the development of the $\delta^{13}C$ isotope sequence in the Sanquan section was different from that in the Jiaodingshan and Xiaogangwan sections. This may be due to the possibility that the real FAD of the *H. brevirameus* in the Xiaogangwan and Jiaodingshan section was lower than the level of the P1 peak, but the earlier occurrences of *H. brevirameus* were not identified in our samples. Another possibility is that the P1 peak in the Sanquan section was misidentified and should be in the lower layer.

The $\delta^{13}C$ isotope sequence in the Jiaodingshan section could be correlated with that in the Liangcun section (Fan et al., 2015b), with three secondary excursions and similar curve evolution. The first excursion was located in the first appearance of the conodont *H. brevirameus*, and the secondary excursion was located in the first appearance of the conodont *P. insculptus,* which is highly consistent within the two sections. The difference is that the range of the peak value was more pronounced than that of the Liangcun section, with the secondary peak value of carbon isotope in the Liangcun section in the range of 1.8‰–2.2‰. The cyclostratigraphic results indicated the duration of the PPCE in the Liangcun and Sanquan sections. The duration of the PPCE in the Sanquan section was 4.37 myr and that in the Liangcun section was 3.75 myr (Ma et al., 2022).

Comparing the $\delta^{13}C$ isotope sequence in the Hongyan section with the sequence in the Jiaodingshan section, it was observed that three secondary excursions were identified in both sections with similar shape curves, and the largest peaks were both in the upper strata (Figure 6). The secondary peak value of the Jiaodingshan section ranged from 2.0‰ to 2.8‰, and the value of the Hongyan section ranged from 1.5‰ to 2.4‰. There is only one conodont zone, *H. brevirameus* zone, that occurs in the Pagoda Formation, and no conodonts were found in the upper formation. The cyclostratigraphic result in the Hongyan section illustrated that the excursion event lasted approximately 3.68 myr (Ma et al., 2022).

To conclude, the carbon isotopic excursion identified in the Pagoda Formation was defined as the Pagoda Positive $\delta^{13}C$ Excursion (PPCE) with three secondary excursions, ranging from 2.0‰ to 3.0‰, which started developing in the same layer with the first appearance of the conodont *H. brevirameus*. The different features of the earliest secondary excursion P1 in the study sections led to the incompleteness of the PPCE. This may be due to the stratigraphic record underlying the Pagoda Formation.

5.4 The cause of the unconformity and its geological implication

The global and regional tectonic movements intensified since the Ordovician, resulting in the gradual disintegration of the Gondwana supercontinent. The marginal Gondwana, such as South China, migrated away from Gondwana to the middle and low latitudes, forming a natural geographically isolated region, which stimulated the evolution of various species. It is speculated that the South China plate of the Late Ordovician, namely, the Late Ordovician Pagoda Formation of the Upper Yangtze Platform, was affected by tectonic movement during its depositional period, resulting in stratigraphic discontinuity and stratigraphic chronological discontinuity between the Pagoda Formation and the underlying formation. The mass generation of methane hydrate is believed to be richer in ^{12}C, and when the global climate cooled, the reserves of methane hydrate in the ocean increased by storing the organic ^{12}C in the methane hydrates or the frozen grounds (e.g., permafrost), leading to an increase in the $\delta^{13}C$ of atmosphere and oceans. This may be related to the cold paleoenvironment of the Upper Yangtze Platform, that is, the South China plate in the Late Ordovician, which was subjected to the Ice Age of the Late Ordovician. Furthermore, the Ordovician radiation caused the organisms to flourish, a process that lasted throughout the whole period of the Ordovician, and the peak of biodiversity before the mass extinction pushed the Ordovician radiation to its climax at the end of the Ordovician (Sepkoski, 1979; Miller and Mao, 1995; Zhan et al., 2013). The statistical results of various marine species showed that two of the three climax acts occurred in the Late Sandbian and Late Katian ages, dominated by brachiopods and other filter feeders, which were in the same period as that examined by this study. During this period, the initial productivity increased, and a large amount of ^{12}C-rich organic carbon was buried relative to inorganic carbon (carbonate), resulting in a positive excursion in the $\delta^{13}C$ value of carbonate.

6 Conclusion

1) The biostratigraphic results showed that three conodont zones were established in the Jiaodingshan and Hongyan sections. They appeared in the *A. tvaerensis*, *H. brevirameus*, and *P. insculptus* zones in ascending order in the Jiaodingshan section, and in the *P. serra*, *Y. jianyeensis*, *H. brevirameus* zones in ascending order in the Hongyan section. Compared with the continuous conodont zones in the Yichang area, the *A. tvaerensis* and *A. superbus* zones were missing.
2) The $\delta^{13}C$ and $\delta^{18}O$ isotope stratigraphic results demonstrated that the $\delta^{13}C$ value ranged from −1.0‰ to 3.0‰ and that the isotopic stratigraphic curve presented three secondary peaks ranging from 2.0‰ to 3.0‰. The characteristics of the $\delta^{13}C$ profile were also present in other areas including Hongyan, Xiaogangwan, Sanquan, and Liangcun. However, the beginning of the event was different. The event in the south and east lasted longer than that in the central and north. This illustrates that the event was more complete in the south and east.
3) The conodont zones absence and the uncompleted $\delta^{13}C$ positive excursion event illustrated a hiatus at the bottom of the Pagoda Formation. The cold paleoenvironment of the Upper Yangtze Platform and Ordovician radiation caused an increase in the initial productivity, and a large amount of ^{12}C-rich organic carbon was buried relative to ^{13}C-rich inorganic carbon, resulting in a positive excursion in the $\delta^{13}C$ value of carbonate.
4) The unconformity could be the channel for hydrocarbon migration or for high-quality oil and gas reservoirs being developed and preserved under the unconformity surface.

Data availability statement

The original contributions presented in the study are included in the article/Supplementary Material, further inquiries can be directed to the corresponding author.

Author contributions

RF and YL performed the data analysis; FZ and YS performed the validation; SD performed the conceptualization; XL and ZQ performed the methodology. XM performed the original draft, review and editing. All authors contributed to the article and approved the submitted version.

Funding

The authors declare that this study received funding from PetroChina Basin Research Program (Grant No. 119063hx00080b18) and Study on Formation Evolution and Dynamic Mechanism of Middle and Lower Assemblage in Superimposed Basin Project (Grant No. 2023ZZ0201). The authors declare that this study received funding from the China National Petroleum Corporation. The funder was not involved in the study design, collection, analysis, interpretation of data, the writing of this article or the decision to submit it for publication.

Acknowledgments

Thanks to all the staff members in the Laboratory of Geological Sciences of RIPED, especially the Stratigraphy and Palaeontology laboratory who provided help in the outcrops and indoor research. Isotope Laboratory of the Nanjing Institute of Geology and Palaeontology, Chinese Academy of Sciences offered help with conodont fossil analysis.

Conflict of interest

Author XM, SD, YL, RF, and YS were employed by PetroChina. Author XL was employed by PetroChina Changqing Oilfield Company. Author ZQ was employed by PetroChina Changqing Oilfield Company.

The remaining author declares that the research was conducted in the absence of any commercial or financial relationships that could be construed as a potential conflict of interest.

Publisher's note

References

An, T. X., Du, G. Q., and Gao, Q. Q. (1981). *Ordovician conodont biostratigraphy in Huanghuachang, Yichang, Hubei*. Beijing, China: Science Press, 105–113.

An, T. X., Du, G. Q., and Gao, Q. Q. (1985). *The Ordovician conodont study in Hubei*. Beijing, China: Geological Publishing, 1–64.

An, T. X. (1987). *The early Paleozoic conodonts in South China*. Beijing, China: Peking University Press, 1–238.

An, T. X., and Zheng, Z. C. (1990). *Conodonts in ordos basin and adjacent area*, 12–132. Beijing, China: Science Press, 162–173.

Anderson, T. F., and Arthur, M. A. (1983). Stable isotopes of Oxygen and Carbon and their application to sedimentology and palaeoenvironmental problems. Society of Economic Paleontologists and Mineralogists. *Short. Course* 10, 155–159. doi:10.2110/scn.83.01.0000

Bathurst, R. G. C. (1972). Carbonate sediments and their diagenesis. *Dev. Sedimentology* 12 (1), 1–658. doi:10.1016/0025-3227(72)90056-4

Bergström, S. M. (1982). Biostratigraphy, evolutionary relationship, and biostratigraphic significance of Ordovician platform conodonts. *Fossils Strata* 15, 35–58.

Bergström, S. M., Chen, X., Schmitz, B., Young, S., Rong, J. Y., and Saltzman, M. R. (2009). First documentation of the ordovician Guttenberg $\delta^{13}C$ excursion (GICE) in asia: chemostratigraphy of the Pagoda and yanwashan formations in southeastern China. *Geol. Mag.* 146, 1–11. doi:10.1017/s0016756808005748

Bergström, S. M., and Ferretti, A. (2017). Conodonts in ordovician biostratigraphy. *Lethaia* 50, 424–439. doi:10.1111/let.12191

Brand, U., and Veizer, J. (1980). Chemical diagenesis of a multicomponent carbonate system-1: trace elements. *J. Sedimental Petroleum* 50, 1219–1236. doi:10.1306/212f7bb7-2b24-11d7-8648000102c1865d

Brasier, M. D., Magaritz, M. M., Corfield, R., Luo, H. L., Wu, X. C., Qu, Y. L., et al. (1990). The carbon and oxygen-isotope record of the Precambrian-Cambrian boundary interval in China and Iran and their correlation. *Geol. Mag.* 127 (4), 319–332. doi:10.1017/s0016756800014886

Brasier, M. D., Shields, G., Kuleshov, V. N., and Zhegallo, E. A. (1996). Integrated chemo- and biostratigraphic calibration of early animal evolution: neoproterozoic–early Cambrian of southwest Mongolia. *Geol. Mag.* 133, 445–485. doi:10.1017/s0016756800007603

Chen, X., Mitchell, C. E., Zhang, Y. D., Bergström, S. M., Winston, D., and Paris, F. (1997). Capsaicin and carbon dioxide act by distinct mechanisms on sensory nerve terminals in the cat cornea. *Acta Palaeontol. Sin.* 4, 23–29. doi:10.1016/s0304-3959(96)03256-3

Chen, X. Y. (1994). Middle ordovician conodont biostratigraphy in tudiao, yanhe. *Guizhou Geol.* 3, 218–223.

Dilliard, K. A., Pope, M., Coniglio, M., Hasiotis, S., and Lieberman, B. (2007). Stable isotope geochemistry of the lower cambrian sekwi formation, northwest territories, Canada: implications for ocean chemistry and secular curve generation. *Palaeogeogr. Palaeoclimatol. Palaeoecol.* 256, 174–194. doi:10.1016/j.palaeo.2007.02.031

Ding, L. S., Chen, M. J., Cao, H. H., Zhang, J. H., Bao, D. X., Yang, Y. L., et al. (1993). *Chapter 2, the Ordovician conodont biostratigraphy and paleogeography*. Beijing, China: Science Publication, 1–100.

Fan, R., Bergström, S. M., Lu, Y. Z., Zhang, X. L., Zhang, S. B., Li, X., et al. (2015b). Upper ordovician carbon isotope chemostratigraphy on the Yangtze platform, southwestern China: implications for the correlation of the Guttenberg $\delta^{13}C$ excursion (GICE) and paleoceanic change. *Palaeogeogr. Palaeoclimatol. Palaeoecol.* 433, 81–90. doi:10.1016/j.palaeo.2015.05.016

Fan, R., Lu, Y. Z., Zhang, X. L., Zhang, S. B., Wang, Z. H., Li, X., et al. (2015a). Ordovician conodont biostratigraphy of the ordovician Liangcun section in Guizhou province, South China. *J. Stratigr.* 39 (1), 15–32. doi:10.19839/j.cnki.dcxzz.2015.01.002

Glumac, B., and Spivak-Birndord, M. L. (2002). Stable isotopes of carbon as an invaluable stratigraphic tool: an example from the Cambrian of the northern Appalachians, USA. *Geology* 30 (6), 563–566. doi:10.1130/0091-7613(2002)030<0563:siocaa>2.0.co;2

Hennissen, J., Vandenbroucke, T. R. A., Chen, X., Tang, P., and Verniers, J. (2016). The Dawangou auxiliary GSSP (Xinjiang autonomous region, China) of the base of the upper ordovician series: putting global chitinozoan biostratigraphy to the test. *J. Micropalaeontology* 29, 93–113. doi:10.1144/0262-821x09-005

Jiang, H. C., and An, T. X. (1985). Ordovician conodont biostratigraphy in South east Sichuan. *Acta Micropalaeontologica Sin.* 1, 14. 27+110–112.

Kaufman, A. J., and Knoll, A. H. (1995). Neoproterozoic variations in the C-isotopic composition of seawater: stratigraphic and biogeochemical implications. *Precambrian Res.* 73, 27–49. doi:10.1016/0301-9268(94)00070-8

Li, D., Ling, H. F., Jiang, S. Y., Pan, J. Y., Chen, Y. Q., Cai, Y. F., et al. (2009). New carbon isotope stratigraphy of the ediacaran cambrian boundary interval from SW China: implications for global correlation. *Geol. Mag.* 146 (4), 465–484. doi:10.1017/s0016756809006268

Li, J. C., Wan, J. F., Liu, H. M., Jurado, M. J., He, Y. X., Yuan, G. J., et al. (2022). Stability analysis of a typical salt cavern gas storage in the jintan area of China. *Energies* 15 (11), 4167–4189. doi:10.3390/en15114167

Lin, B. Y., Qiu, H. R., and Xu, C. C. (1984). New observations of ordovician strata in shetai district of urad front bannor, nei mongol (inner Mongolia). *Geol. Rev.* 30 (2), 95–105. doi:10.16509/j.georeview.1984.02.001

Ma, X. Y., Lu, Y. Z., Zhong, L., Fan, R., Li, X., and Deng, S. H. (2019a). Carbon isotope characteristics of the ordovician Pagoda Formation at the sanquan section in nanchuan, chongqing and its correlation. *J. Stratigr.* 43 (1), 18–27. doi:10.19839/j.cnki.dcxzz.2019.01.002

Ma, X. Y., Fan, R., Lu, Y. Z., Luo, Z., Deng, S. H., and Zhang, F. (2019b). Middle-Upper Ordovician conodont sequence and its geological significance in Nanchuan area, Chongqing. *Acta Pet. Sin.* 40, 577–586. doi:10.7623/syxb201905007

Ma, X. Y., Deng, S. H., Lu, Y. Z., Wu, H. C., Luo, Z., Fan, R., et al. (2019c). Astrochronology of the upper ordovician Pagoda Formation, South China and its geological implications. *Earth Sci. Front.* 26, 281–291. doi:10.13745/j.esf.sf.2019.3.8

Ma, X. Y., Ogg, J., Lu, Y. Z., Fan, R., Huang, C. J., Luo, Z., et al. (2022). The upper ordovician Pagoda positive $\delta^{1}3C$ excursion (PPCE) on the upper Yangtze platform, South China. *J. Asian Earth Sci.* 240, 105373. doi:10.1016/j.jseaes.2022.105373

MacDonald, F. A., Hodgin, E., Crockford, P. W., Crockford, P. W., and Delano, J. W. (2017). Bridging the gap between the foreland and hinterland II: geochronology and tectonic setting of Ordovician magmatism and basin formation on the Laurentian margin of New England and Newfoundland. *Am. J. Sci.* 317, 555–596. doi:10.2475/05.2017.02

Miller, A. I., and Mao, S. G. (1995). Association of orogenic activity with the Ordovician radiation of marine life. *Geology* 23, 305–308. doi:10.1130/0091-7613(1995)023<0305:aooawt>2.3.co;2

Mu, E. Z., Zhu, Z. L., Cheng, J. Y., and Rong, J. Y. (1987). Ordovician stratigraphy in shuanghe, changning. *J. Stratigr.* 2, 105–121.

Ogg, J. G., Christopher, R. S., Hou, M., Chen, A. Q., Ogg, G. M., and Zhong, H. T. (2019). Global paleogeography through the proterozoic and phanerozoic: goals and challenges. *Acta Geol. Sin.* 93 (1), 59–60. doi:10.1111/1755-6724.14245

Peng, J., Han, H. D., Xia, Q. S., and Li, B. (2018). Fractal characterization and genetic mechanism of micro-pore structure in deeply buried tight sandstone reservoirs: a case study of kalpintag Formation in shuntuoguole area, Tarim Basin. *Acta Pet. Sin.* 39 (07), 775–791. doi:10.7623/syxb201807005

Rong, J. Y., Chen, X., and Harper, D. A. (2000). Proposal of a GSSP candidate section in SouthSouth China for a new hirnantian boundary Stratotype. *J. Stratigr.* 3, 176–181.

Sepkoski, J. J. J. (1979). A kinetic model of Phanerozoic taxonomic diversity II. Early Phanerozoic families and multiple equilibria. *Paleobiology* 5, 222–251. doi:10.1017/s0094837300006539

Sepkoski, J. J., and Sheehan, P. M. (1983). *Biotic interactions in recent and fossil benthic communitie*. New York, USA: Plenum Press, 673–717.

Sheng, X. F., and Ji, Z. L. (1986). The geological time of the Pagoda Formation. *Proc. Stratigr. Palaeontol.* 3, 1–36.

Sheng, X. F., and Ji, Z. L. (1984). The sedimentary environment and geological time of the Pagoda Formation. *Chin. Geol.* 11, 31–32.

Wan, X. M., Zhou, X. Q., Liang, J. Q., Wu, S. G., Lu, J. G., Wei, C. L., et al. (2022). Well-logging constraints on gas hydrate saturation in unconsolidated fine-grained reservoirs in the northern South China sea. *Energies* 15 (23), 9215–9237. doi:10.3390/en15239215

Wang, C. Y. (1993). *Conodonts of the lower Yangtze Valley-An index to biostratigraphy and organic maturity*. Beijing, China: Science Press, 1–326.

Wang, X. F., and Ni, S. J. (1987). *Biostratigraphy of the Yangtze gorge area (2) early palaeozoic era*. Beijing, China: Geological Publishing House, 386–448.

Wang, Y. Y., Chen, J. F., Pang, X. Q., Shen, W. B., Zhang, B. S., Zhang, G. Q., et al. (2018a). Ordovician hydrocarbon charging characteristics and migration direction in Tazhong area. *Acta Pet. Sin.* 39 (01), 54–68. doi:10.7623/syxb201801005

Wang, Z. H., Qi, Y. P., and Wu, R. C. (2011). *Cambrian and ordovician conodont in China*. Hefei, China: Press of University of Science and Technology of China, 1–388.

Wang, Z. H., Zhen, Y. Y., Ma, H., and Zhang, Y. D. (2017). Middle to upper ordovician conodont succession from the qiliao sections of shizhu, chongqing-revealing a depositional hiatus between lower darriwilian and sandbian. *Acta Palaeontol. Sin.* 56 (1), 37–53. doi:10.19800/j.cnki.aps.2017.01.005

Wang, Z. H., Zhen, Y. Y., Ma, X., and Zhang, Y. D. (2018b). Ordovician conodonts from the kuniutan to Pagoda formations at Chenjiahe and Zhenjin of Yichang, Hubei province, China and their stratigraphic significance. *Acta Micropalaeontologica Sin.* 35 (1), 13–29. doi:10.16087/j.cnki.1000-0674.2018.01.002

Wei, X. S., Ren, J. F., Zhao, J. X., Zhang, D. F., Luo, S. S., Wei, L. B., et al. (2017). Paleo-geomorphologic characteristic evolution and geological significance of the Ordovician weathering crust in eastern Ordos Basin. *Acta Pet. Sin.* 38 (09), 999–1009. doi:10.7623/syxb201709002

Zhan, R. B., Jin, J. S., and Liu, J. B. (2013). Investigation on the great Ordovician biodiversification event (GOBE): review and prospect. *Chin. Sci. Bull. Chin. Ver.* 58, 3357–3371. doi:10.1360/972013-19

Zhao, Z. J., Zhao, Z. X., and Huang, Z. B. (2006). Ordovician conodont zones and sedimentary sequences of the Tarim Basin, Xinjiang, NW China. *J. Stratigr.* 33 (3), 193–203.

Zhu, M. Y., Zhang, J. M., Li, G. X., and Yang, A. H. (2004). Evolution of C isotopes in the cambrian of China: implications for cambrian subdivision and trilobite mass extinctions. *Geobios* 37, 287–301. doi:10.1016/j.geobios.2003.06.001